Canadian Geotechnical Journal
Revue canadienne de géotechnique

Interpolating spatially varying soil property values from sparse data for facilitating characteristic value selection

Journal:	*Canadian Geotechnical Journal*
Manuscript ID	cgj-2017-0219.R1
Manuscript Type:	Article
Date Submitted by the Author:	24-Jun-2017
Complete List of Authors:	Zhao, Tengyuan; City University of Hong Kong, Architecture and civil engineering Montoya-Noguera, Silvana; City University of Hong Kong Phoon, Kok-Kwang; National University of Singapore, Department of Civil & Environmental Engineering Wang, Yu; City University of Hong Kong, Dept of Civil and Architectural Engineering
Keyword:	Reliability-based design, Bayesian compressive sampling, compressive sensing, sparse measurement data, site investigation

Interpolating spatially varying soil property values from sparse data for facilitating characteristic value selection

Tengyuan Zhao[1], Silvana Montoya-Noguera[2], Kok-Kwang Phoon[3] and Yu Wang[4]

[1] PhD Student, Department of Architecture and Civil Engineering, City University of Hong Kong, Tat Chee Avenue, Kowloon, Hong Kong

[2] Research Associate, Department of Architecture and Civil Engineering, City University of Hong Kong, Tat Chee Avenue, Kowloon, Hong Kong

[3] Distinguished Professor, Department of Civil and Environmental Engineering, National University of Singapore, Singapore

[4] Associate Professor, Department of Architecture and Civil Engineering, City University of Hong Kong, Tat Chee Avenue, Kowloon, Hong Kong. (Tel): 852-3442-7605 (Fax):852-3442-0427 (Email): yuwang@cityu.edu.hk (Corresponding author)

Abstract

Limit state design, incorporated into many recent geotechnical design codes, introduces the application of partial or resistance factors to selected characteristic values. Partial or resistance factors are usually set by national standard organizations, while characteristic values of geotechnical parameters are selected by engineers, often based on sparse measurement data combined with subjective engineering experience and judgment. Due to this subjective selection and individual judgment, the characteristic value derived by different engineers from the same dataset may vary greatly, especially when the test data contain significant variability. To address this issue, a new method based on Bayesian compressive sampling (BCS) is proposed in this study. BCS is able to reconstruct a high-resolution geotechnical property profile from sparse measurement data and quantify the uncertainty, e.g. confidence interval (CI) associated with the interpreted profile. The quantified uncertainty in the BCS has a clear statistical meaning: the corresponding confidence level for a CI from the BCS is the expected coverage proportion (i.e. fraction) of the complete profile that falls within the CI, if all data points along depth can be measured to provide the complete profile. This statistical meaning can be used to facilitate objective determination of characteristic values for geotechnical properties.

Keywords: Reliability-based design; Bayesian compressive sampling; compressive sensing; sparse measurement data; site investigation

Introduction

Limit state design methods have been recently incorporated into many geotechnical codes of practice throughout the world, e.g. Eurocode 7 (CEN 2004), AASHTO Bridge Code (AASHTO 1998), and Canadian Highway Bridge Design Code (CHBDC 2014), among others. To achieve a specific target reliability level, the design value is determined by dividing the characteristic strength values by partial factors (e.g. Meyerhof 1995; Fenton and Naghibi 2011; Reddy and Stuedlein 2017) or multiplying the characteristic resistance values by resistance factors. Partial or resistance factors are usually set by national standard organizations and are used to achieve a target level of reliability or safety (although explicit reliability calibration may not be conducted); while the characteristic values of geotechnical parameters are selected by geotechnical engineers. In engineering practice, these characteristic values are often selected based on a limited number of test results, therefore engineering judgment and previous relevant experience are frequently used to select the characteristic values (e.g. Orr 2017).

Because of this subjective selection and individual judgment, the characteristic values, derived by different geotechnical engineers from the same dataset, may vary greatly, especially when the test data are scarce or contain significant variability. For example, Bond and Harris (2008) presented three case studies in which about one hundred engineers were asked to select the characteristic values on the basis of Eurocode 7 from the same set of test data. The case studies dealt with different types of data (SPT blow counts, field vane tests and triaxial tests), different soil types (clays and gravels) and different number of data points (from 25 to above 100 points for profiles of 10 to 30m deep). The selected characteristic values varied greatly, and the maximum characteristic value obtained was about 3 to 5 times greater than the minimum one. Orr (2017) suggested that more guidance is needed to select characteristic values in an objective manner to reduce and properly account for this broad range of interpretation.

Statistical analyses of laboratory and in-situ test results to determine geotechnical parameters for reliability-based design applications have been broadly discussed and recommended in the literature (e.g. Vanmarcke 1977; Phoon and Kulhawy 1999; Baecher and Christian 2003; Fenton and Griffiths 2008; Becker 2010; Gong et al. 2014; Li et al. 2016; Phoon et al. 2016). Although statistical methods are explicitly recommended in some design guides (e.g. Det Norske Veritas 2010), currently the use of such analyses has not been included in some existing design codes, such as Eurocode 7, partially because of the limited number of site specific measurement data and the inherent variability encountered in natural soil deposits (Orr 2017). Furthermore, most of the available statistically based methods for determining the characteristic values of geotechnical parameters focus on point statistics (e.g. mean and coefficient of variation for a previously defined homogeneous soil layer) and hence ignore the spatially varying pattern of soil properties (e.g. Cao and Wang 2014; Wang et al. 2016a; Wang and Aladejare 2016; Wang and Cao 2013).

This paper aims to address these two issues, limited data and inherent spatial variability, and to provide a statistical procedure for an *objective* determination of characteristic value from spatially varying but sparsely measured data. It uses compressive sampling theory to reconstruct the best estimate of a soil property profile from sparse measurement data points (Wang and Zhao 2016) and Bayesian theory to estimate the statistical uncertainty associated with the interpreted profile (Wang and Zhao 2017). The use of the Bayesian framework acknowledges the critical role of engineering judgment but reduces the subjective interpretation uncertainty by quantitatively representing it as prior knowledge (e.g. Cao, Wang and Li 2016; Vick 2002; Wang and Aladejare 2015; Wang et al. 2016b).

This paper first presents an interpretation of the statistical meaning of the confidence interval for random field data. Then it reviews the formulation of BCS and uses it to provide average and confidence interval profiles, given only sparsely measured but spatially varying geotechnical data. Note that the measurement data of soil properties obtained in geotechnical engineering are usually sparse and limited, particularly for small or medium sized projects. An important question when interpreting sparse data in geotechnical practice is: how does the profile interpreted from sparse data compare with the measured profile, if it is possible to measure the geotechnical data with a small interval and a high resolution? This paper shows that the confidence interval (CI) profile quantified in BCS has a clear statistical meaning, which may be used to address this question and to facilitate determination of characteristic values in engineering practice. For illustration, the proposed BCS procedure is applied to a real case of CPT data and the selection of the characteristic value of effective friction angle.

This paper addresses the characteristic value only from a purely *statistical* perspective, although characteristic value may be related to the extent of failure zone governing the behavior of the structure at the limit state. For example, some researchers have argued that the characteristic value is related to the concept of a mobilized strength along the critical slip surface (Ching and Phoon 2013a, 2013b; Ching et al. 2014, 2016a) or a mobilized modulus over a domain influenced by the structure at the limit state (Ching et al. 2016b). As the limit state of a geo-structure is problem dependent, and a realistic assessment of the characteristic value in the context of spatial variability where non-classical failure mechanisms can emerge is less straightforward, the extent of failure zone governing the behavior of the structure at the limit state is not considered in this paper.

Coverage proportion of confidence interval profiles

The confidence interval (CI), which may be used to quantify uncertainty, is more informative than simply reporting a point estimate (e.g. Phoon and Ching 2014). CI is an interval estimation of a parameter of interest which gives a confidence level that the true parameter falls within the estimated CI. To evaluate the confidence interval, analytical equations can be used when the distribution of the data is known. For example, for normally distributed data with a known mean (μ) and standard deviation (σ), the CI for a confidence level α, denoted as CI_α, is expressed as:

$$\mathrm{CI}_\alpha = \mu \pm z_{(1-\alpha)/2}\sigma \qquad (1)$$

where $z_{(1-\alpha)/2} = -\Phi^{-1}[(1-\alpha)/2)]$ and $\Phi^{-1}(\cdot)$ is the inverse standard normal cumulative distribution function. Note that the lower bound of Equation (1) or its variants (i.e. μ minus a factored σ) has been proposed in literature, e.g. Schneider and Schneider (2013) and Orr (2017) as characteristic value at a given depth or for a homogeneous soil layer in Eurocode 7.

For spatially varying data, such as random field samples (RFSs), the values vary along a spatial dimension (e.g. depth), hence the mean and CI_α also vary along this spatial dimension, e.g. profiles varying with depth. For a given random field with known μ and σ, CI_α profiles (i.e. variations of CI_α with depth) can be generated analytically by applying Equation (1) to different depths. For example, the $\mathrm{CI}_{90\%}$ profiles can be obtained by substituting α=90% to Equation (1) for different depths of interest.

CP_α of CI_α profiles for random field data

The coverage proportion (CP_α) of a soil property profile $\boldsymbol{f}$, e.g. a RFS, that falls within a CI_α profile with a confidence level (α) is defined as (e.g. Marra and Wood 2012; Nychka 1988; Wahba 1983):

$$\mathrm{CP}_\alpha = \frac{1}{\mathrm{N}}\sum_{k=1}^{\mathrm{N}}[\mathrm{I}(f_k \in \mathrm{CI}_\alpha)] \tag{2}$$

where N is the total number of data points in the soil property profile $\boldsymbol{f}$, and $\mathrm{I}(\cdot)$ is the indicator function. $\mathrm{I}(\cdot)$ equals to unity if a data point f_k (k = 1, 2, …, N) is within the upper and lower bounds of CI_α, and otherwise, it is zero. Note that the expected value of CP_α is equal to α (Wahba 1983). For example, $CI_{95\%}$ implies that 95% of all data points are expected to fall within the upper and lower bounds given by $CI_{95\%}$, i.e. $CP_{95\%}$ = 95%. The coverage proportion has been evaluated for CI_α profiles obtained from smoothing functions (e.g. Nychka 1988; Wahba 1983) and generalized additive models (e.g. Marra and Wood 2012). In this section, the procedure to evaluate the CP_α of a RFS that falls within a CI_α profile is firstly explained. Then the procedure is illustrated with simulated random field data. This section is meant to explain the definition and evaluation of CP_α, and it paves the way for the next section where CP_α will be evaluated for the CI_α profiles obtained from the BCS method with a limited number of measurement data as input.

Note that if the random field has no correlation (i.e. the data points over the depth are independent), the probability distribution of CP_α follows a binomial distribution because of the indicator function in Equation (2) (e.g. De Veaux et al. 2014; Efron and Tibshirani 1993). Hence, the average CP_α is equal to α, and the variance is equal to $\alpha(1-\alpha)/\mathrm{N}$. The shape of the distribution of CP_α is symmetric (i.e. zero skewness) for α=0.5 and it is negatively skewed as α approaches 1 (De Veaux et al. 2014). The distribution of CP_α tends to the normal distribution as N increases and α approaches 0.5. De Veaux et al. (2014) suggest that a normal distribution gives a good approximation of the binomial distribution if $N\alpha \geq 10$ and $N(1-\alpha) \geq 10$.

Simulation of random field examples

For illustration, a 1D stationary Gaussian random field is used to represent a soil property X profile. Random field samples (RFSs) are generated using a truncated Karhunen-Loève (KL) expansion. Truncated KL expansion has been increasingly studied and used in simulating 1D random processes in recent years (e.g. Zhang and Ellingwood 1994; Phoon et al. 2002; Phoon et al. 2005; Li et al. 2014). The following parameters were used: mean $\mu_X = 30$, standard deviation $\sigma_X = 2$ and an exponential correlation function, i.e. $\rho_{i,j} = \exp\left(-\frac{2\left|d_{X_i}-d_{X_j}\right|}{\lambda_c}\right)$, where d_{X_i} and d_{X_j} are the depths of two X data points X_i and X_j, respectively, and λ_c is the correlation length taken as 2m in this example. The soil layer thickness (h) is taken as 20.44m and the profile has a resolution of 0.04m. Hence there are N = 512 points for each RFS. Note that only one homogeneous soil layer (rather than several soil layers) with a thickness of 20.44m is considered in this illustrative example. Stratification therefore is not needed in this example. For the truncated KL expansion, 200 KL terms are used. Note that 200 terms are able to preserve 98.2% of the total variance of the random field in terms of the sum of 200 eigenvalues and the sum of all eigenvalues in this example. Therefore, it accurately represents the prescribed random field (e.g. Phoon et al. 2002). The number of RFS (N_s) generated is 1000. All RFSs generated are shown in Figure 1 in light gray. Additionally, the profile of the mean values, evaluated as the average of all N_s values at each depth, is also shown.

Probability distribution of CP_α for CI_α profiles

The CI_α profiles over depth are constructed using Equation (1) with a given confidence level α. For example, given α=95%, the $CI_{95\%}$ profiles are obtained with the 2.5th and 97.5th percentiles from Equation (1) and are shown in Figure 1 by two dotted lines. In each subplot of this figure, one RFS is shown in black solid line to illustrate the evaluation of $CP_{95\%}$. For each one of these samples, the coverage proportion of the RFS profile that is within the $CI_{95\%}$ profiles (i.e. between the two dotted lines in Figure 1) is evaluated. The $CP_{95\%}$ values for the three RFSs presented in Figure 1 are 94.5%, 94.9% and 96.1%, respectively.

The CP_α values are evaluated for all N_s = 1000 RFSs and for different α values ranging from 50% to 95%. Statistical analysis is performed for the CP_α values obtained, and the results are shown as box-and-whiskers plots for different α values in Figure 2b. The box is constructed with the inter-quartile range, IQR = 25% - 75% percentiles, and the whiskers show the minimum and maximum values within 1.5IQR. The maximum and minimum CP_α values among all N_s RFSs are shown by crosses in Figure 2, and the mean CP_α values are shown with circles. Figure 2 also includes a 1:1 line in each subplot. The mean CP_α values for the α value varying from 50% to 95% all plot along the 1:1 line, and the average CP_α is equal to α. The CI_α profiles can be statistically interpreted as the upper and lower bounds of an interval where the expected coverage proportion (i.e. fraction) of a RFS (i.e. a spatially variable soil property X profile) that falls within the interval is α.

Note that, although the expectation of CP_α is α, the CP_α value for each RFS may vary significantly, as shown in Figure 2. When the CP_α values are greater than the α values, a relatively large proportion of the RFS fall within the interval. In contrast, when the CP_α values are smaller than the α values, a relatively large proportion of the RFS fall outside the

CI_α profiles. For example, for the worst case in Figure 2b, the smallest $CP_{50\%}$ value is close to 20%. This means that, besides the 50% expected, an additional 30% of the RFS falls outside the $CI_{50\%}$ profiles. For all N_s = 1000 RFSs, less than 3% of RFSs present a $CP_{95\%}$ lower than 85.5% (i.e. a relative difference of 10% on the expected value). In contrast, for $CP_{50\%}$, about 30% of RFSs are below 45% (i.e. the same 10% difference). As the confidence level increases, the variability of the CP values decreases, as shown by the decreasing size of the box and whiskers as the α value approaches unity. In addition, the mean and median CP_α values (shown with a line inside the box in Figure 2) are similar for α equal 50%, but the median CP_α value is slightly larger than the mean CP_α value for high α values. In other words, the CP_α results are symmetric, i.e. present zero skewness, for α close to 0.5, but develop a negative or left skewness as α approaches unity. This is similar to the effect of small N values when the random field has no correlation and the CP_α values follow a binomial distribution (De Veaux et al. 2014).

Effect of different correlation length in random field

The same procedure as described previously was used for generating RFSs with various λ_c values. Figures 2a and 2c show the box-and-whiskers plots of the corresponding CP_α results for λ_c = 0.5m and 5m, respectively. For all the cases, the mean CP_α is equal to α, although the results present more variability for the case of λ_c = 5m. The variability of CP_α increases as the correlation length increases, as shown by the size of the box and the length of the whiskers in Figure 2. Compared to the case of λ_c=2m, the CP_α results for the case of λ_c = 0.5m are more concentrated around α. The decrease in the CP_α variability as α increases is less visible for the case of λ_c = 0.5m. Also, for the case of λ_c = 0.5m, the median CP_α is also equal to α, and all CP_α distributions appear to be symmetric. In contrast, for the case of λ_c =

5m shown in Figure 2c, the variability of CP_α increases, and distributions are markedly skewed for high α values. It can be seen that, for α greater than 0.7, the median CP_α values are greater than α. Thus more than 50% of RFSs have a CP_α equal to or greater than α.

A total of eight different λ_c values were tested ranging from 0.1 to 10m. This range of correlation length is consistent with those of geotechnical properties reported in literature (e.g. Phoon and Kulhawy 1999). The box plots of the CP_α results are shown in Figure 3a for three α values: 50%, 80% and 95%. For all results, the CP_α mean values are equal to the corresponding α values, independent of either λ_c or α. However, the median values are greater than the mean values for high confidence levels, and the difference between mean and median values increases with the correlation length. Furthermore, the size of the boxes in Figure 3a increases with λ_c, suggesting that the variability of the CP_α results increases with λ_c.

To visualize the effect of the correlation length and the confidence level on the variation of CP_α results, Figure 3b shows the standard deviation evaluated for CP_α ($\sigma_{CP\alpha}$) as a function of α. When there is no correlation in the random field, the standard deviation is evaluated as $\sigma_{CP\alpha}= \sqrt{\alpha(1-\alpha)/N}$, as for the binomial distribution, and shown by a solid line in Figure 3b. A random field with no correlation was tested and the results obtained for $\sigma_{CP\alpha}$ agree well with the analytical solution. When there is no correlation, the $\sigma_{CP\alpha}$ reaches its maximum for α = 0.5. However, as λ_c increases, the maximum value of $\sigma_{CP\alpha}$ occurs at a relatively large α value. For λ_c equal to 10m, a maximum $\sigma_{CP\alpha}$ of about 0.18 is found at α = 0.65. In general, the $\sigma_{CP\alpha}$ increases as λ_c value increases. But this increase is more pronounced for relatively small α values. For α = 0.95, the $\sigma_{CP\alpha}$ is quite small, even for high correlation lengths because the upper bound of $CP_{95\%}$ = 1 is reached in many cases.

It is worth noting that the aforementioned CI_α profiles are obtained from a prescribed random field with known parameters. In geotechnical engineering practice, if a soil property profile is represented by a random field, its random field parameters, such as mean, standard deviation and correlation function, are often difficult to estimate from measurement data, especially the last two parameters. This is in part because the measurement data of soil properties are usually limited and sparse. To address this difficulty, a Bayesian compressive sampling method has been recently developed to statistically interpret the sparse measurement data points for providing the best estimate and CI_α profiles of the soil properties (Wang and Zhao 2017), as briefly reviewed in the next section.

Review of Bayesian compressive sampling (BCS)

Bayesian compressive sampling (BCS) is a coupling of compressive sampling or sensing (CS) and the Bayesian method to reconstruct the average and standard deviation profiles of a soil property profile from only partial information of the profile, i.e. sparse measurement data points (e.g. Ji et al. 2008; Wang and Zhao 2017). CS, mainly applied in electrical engineering and computer science, exploits sparsity, or compressibility, in many real-world signals (e.g. Candès et al. 2006; Candès and Wakin 2008). A signal, denoted as a column vector $\boldsymbol{f}$ with a length of N, is defined as the variation of a physical quantity with time or space. "Compressibility" means that a signal $\boldsymbol{f}$ can be represented concisely as a weighted summation of a proper type of basis functions, such as wavelet functions. In the mathematical formulation of CS, $\boldsymbol{f}$ is expressed as follows:

$$\boldsymbol{f} = \mathbf{B}\boldsymbol{\omega} \tag{3}$$

where $\mathbf{B}$ is a N×N orthonormal matrix composed of columns of pre-specified basis functions, and $\boldsymbol{\omega}$ is the corresponding weight coefficient vector with a length of N. Because of the compressibility of signals, most entries in $\boldsymbol{\omega}$ are near to zero. Thus, $\boldsymbol{f}$ can be reconstructed by identifying and estimating the weight coefficients with significant value using the sparse measurement data vector $\boldsymbol{y}$ that has a length of M, where M<N, as follows:

$$\boldsymbol{y} = \boldsymbol{\Psi}\boldsymbol{f} = \mathbf{A}\boldsymbol{\omega} \tag{4}$$

where $\boldsymbol{\Psi}$ is a M×N matrix and represents the locations of components $\boldsymbol{y}$ in $\boldsymbol{f}$. $\mathbf{A} = \boldsymbol{\Psi}\mathbf{B}$ is also a M×N matrix (Wang and Zhao 2016). Exploiting sparsity, the resulting underdetermined system of linear equations, i.e. Equation (4), can be solved by various existing efficient algorithms (e.g. Foucart and Rauhut 2013). For example, Wang and Zhao (2017) used a Bayesian method to statistically reconstruct the signal $\hat{\boldsymbol{f}}$, which is an approximation of $\boldsymbol{f}$. Mathematically, $\hat{\boldsymbol{f}}$ is defined by:

$$\hat{\boldsymbol{f}} = \mathbf{B}\boldsymbol{\omega}_s \tag{5}$$

where $\boldsymbol{\omega}_s$ is the approximate weight coefficient vector with a length of N, and all components are set to zero except for the S non-trivial components (S<<N). Following the Bayesian framework (Wang and Zhao 2017), the posterior marginal distribution of $\boldsymbol{\omega}_s$ derived from $\boldsymbol{y}$ follows a multivariate Student t distribution with a degree of freedom equal to $2c_n$ and a scale

matrix of $(d_n/c_n)\mathbf{H}$. The mean and covariance matrix of $\boldsymbol{\omega_s}$ (i.e. $\mu_{\boldsymbol{\omega_s}}$ and $\mathbf{COV}_{\boldsymbol{\omega_s}}$, respectively) are expressed as:

$$\mu_{\boldsymbol{\omega_s}} = \mathbf{H}\mathbf{A}^{\mathrm{T}}\boldsymbol{y}$$
$$\mathbf{COV}_{\boldsymbol{\omega_s}} = \frac{d_n\mathbf{H}}{c_n - 1} \tag{6}$$

where $\mathbf{H} = (\mathbf{A}^{\mathbf{T}}\mathbf{A} + \mathbf{D})^{-1}$, $c_n = \mathrm{M}/2 + c_0$ and $d_n = \left(\boldsymbol{y}^{\boldsymbol{T}}\boldsymbol{y} - \mu_{\boldsymbol{\omega_s}}^{\mathrm{T}}\mathbf{H}^{-\mathbf{1}}\mu_{\boldsymbol{\omega_s}}\right)/2 + d_0$. c_0 and d_0 are small non-negative constants, e.g. $c_0 = d_0 = 10^{-4}$, $\mathbf{D}$ is a N×N diagonal matrix with components $\mathrm{D}_{i,i} = \alpha_i$ and α_i are unknown non-negative coefficients. Note that Equation (6) only depends on α_i and requires an iterative algorithm (e.g. the maximum likelihood estimation) to obtain the most probable value of α_i. Only the α_i values corresponding to the S (S<<N) non-trivial coefficients in $\boldsymbol{\omega}_s$ need to be estimated in BCS, hence bypassing the possible problem caused by high dimensionality. The number S of coefficients needed is obtained by an iteration procedure using cosine similarity (Wang and Zhao 2017).

Because $\boldsymbol{\omega_s}$ follows a multivariate Student t distribution and Equation (5), $\hat{\boldsymbol{f}}$ is also derived as a random vector following a multivariate Student t distribution (e.g. Ang and Tang 2007; Fenton and Griffiths 2008), with $2c_n$ degree of freedom, mean $\mu_{\hat{\boldsymbol{f}}}$ and scale matrix $(d_n/c_n)\mathbf{B}\mathbf{H}\mathbf{B}^{\mathrm{T}}$. The mean and covariance of $\hat{\boldsymbol{f}}$ (i.e. $\mu_{\hat{\boldsymbol{f}}}$ and $\mathbf{COV}_{\hat{\boldsymbol{f}}}$, respectively) are derived as:

$$\mu_{\hat{f}} = \mathbf{B}\mu_{\omega_s}$$

$$\mathbf{COV}_{\hat{f}} = \mathbf{BCOV}_{\omega_s}\mathbf{B}^{\mathrm{T}} = \frac{d_n}{c_n - 1}\mathbf{BHB}^{\mathrm{T}} \tag{7}$$

The BCS procedure has been implemented by a package of user functions in MATLAB (Mathworks, 2016). Only the sparse measurement data from site characterization are required to obtain the mean and CI profiles of soil properties of interest.

In the following section, the BCS method is used to provide the best estimate of a complete soil property profile from sparse measurement data and construct the associated CI profiles. A statistical meaning of the CI profiles obtained from BCS is proposed: the corresponding confidence level for a CI profile from BCS is the expected coverage proportion (i.e. fraction) of the complete profile that falls within the CI, if all data points along depth can be measured to provide the complete profile. The statistical meaning of the BCS CI profiles is similar to that of the CI profiles for random field data shown in the section "Coverage proportion of confidence interval profiles". The statistical meaning of the BCS CI profiles will be evaluated systematically in the next section.

Coverage proportion of the BCS confidence interval profiles

Construction of CI profiles obtained from BCS with sparse measurement data as input

As $\hat{\boldsymbol{f}}$ follows a multivariate Student t distribution (Wang and Zhao 2017), the upper and lower bounds of the confidence interval are defined as (e.g. Taboga 2012):

$$\mathbf{CI}_{\alpha} = \mu_{\hat{f}} \pm t_{(1-\alpha)/2,2c_n}\sqrt{(2c_n-2)/2c_n}\sqrt{\mathbf{diag}\left(\mathbf{COV}_{\hat{f}}\right)} \tag{8}$$

where $t_{(1-\alpha)/2,2c_n}$ is the Student t factor for a confidence level α and a degree of freedom $2c_n$, $\sqrt{(2c_n-2)/2c_n}$ is a scaling factor; and $\sqrt{\mathbf{diag}\left(\mathbf{COV}_{\hat{f}}\right)}$ is a column vector composed of the square root of the diagonal elements of $\mathbf{COV}_{\hat{f}}$. Note that $\mathbf{CI}_{\boldsymbol{\alpha}}$ is composed of two column vectors, which correspond to the upper and lower bounds of the two-tailed data distribution at various depths (e.g. for α = 90%, the lower and upper bounds are the 5th and 95th percentiles, respectively).

Consider, for example, using BCS to reconstruct the three RFSs shown in Figure 1 with only M=20 measurement data points from each RFS as input (i.e. the sparse measurement data $\boldsymbol{y}$). Figure 4 shows the M=20 measurement data points by open circles. The best estimate (i.e. mean) of the complete soil property X profile and 95% CI profiles are shown in Figure 4 as dashed and dotted lines, respectively. Additionally, the original and complete RFS profile is shown by a solid line in Figure 4 for comparison. Figure 4 shows that, although the best estimate (i.e. the dashed line) does not go exactly through the measurement data points (i.e. open circles), it follows a trend similar to that of these data points and the original and complete RFS profiles. This suggests that the soil property X profile reconstructed from BCS is consistent with the original variation of X with depth, even when only a limited number of measurement data points (e.g. 20 from a total of 512 data points) are used as input.

Some local variations of the original profile are not reconstructed in the best estimate profile. This is because the number of measurement data is too limited (i.e. M=20≪N=512), hence the statistical uncertainty is quite significant. The statistical uncertainty can be explicitly and objectively quantified by the covariance calculated in Equation (7) and the CI profiles calculated with Equation (8). For example, the bounds of the $CI_{95\%}$ profiles are shown in Figure 4 by two dotted lines. Similar to the CI profiles for random field data discussed previously, the BCS CI profiles have a statistical meaning: the corresponding confidence level for a BCS CI profile is the expected coverage proportion (i.e. fraction) of the complete profile that falls within the CI, if all data points over depth can be measured to provide the complete profile. In other words, although some details of the original profile are not reflected by the best estimate from only 20 measured data points, on average around 95% of all local variations of the original profile fall within the $CI_{95\%}$ upper and lower bounds. For example, the $CP_{95\%}$ values of the three original RFSs shown in Figure 4 are 94.9%, 94.1% and 96.3%, respectively. Hence, about 95% of the three original RFSs shown in Figure 4 fall within the $CI_{95\%}$ upper and lower bounds. Recall that, in the subsection "Probability distribution of CP_α for CI_α profiles", the similar $CP_{95\%}$ values evaluated for the full set of random field data were 94.5%, 94.9% and 96.1%, respectively. The difference is less than 1% and quite minor.

Probability distribution of CP_α for BCS CI_α profiles

To evaluate the probability distribution of CP_α for the BCS CI_α, the BCS method is used to construct each of the N_s = 1000 RFSs shown in Figure 1, using a limited number, e.g. M=20, of measurement data points from each RFS as input (i.e. $\boldsymbol{y}_i$, i = 1, 2, …, N_s). This leads to a total of 1000 best estimates and CI profiles obtained from BCS. Each of the 1000 RFSs is used as the original and complete soil property X profile, which is compared with the corresponding best estimate and CI profiles obtained from each BCS interpretation. The coverage proportion (CP_α) of each of the 1000 RFSs that falls within the corresponding BCS CI_α profiles was evaluated for different α values ranging from 50 to 95%.

Figure 5a to 5c show histograms of $CP_{50\%}$, $CP_{80\%}$ and $CP_{95\%}$, respectively, when M = 20 (i.e. 20/512=3.9% or less than 4% of the complete profile is measured). The mean $CP_{50\%}$, $CP_{80\%}$ and $CP_{95\%}$ values are shown in Figures 5a to 5c as 0.54, 0.79, and 0.92, respectively. These mean CP values are quite close to their respective α values (i.e. 0.5, 0.8 and 0.95, respectively). Therefore, the confidence level may be interpreted as the expected coverage proportion of the original and complete profile that falls within the corresponding BCS CI profiles, if the original and complete profile can be measured. Additionally, similar to the random field data discussed in the section "Coverage proportion of confidence interval profiles", the CP probability distribution is close to symmetric when α = 50% (see Figure 5a). As α increases and approaches unity, the distribution becomes less symmetric and presents a negative skewness (see Figures 5b and 5c). Similar to Figure 2, Figure 6a shows box-and-whiskers plots for CP_α with various α values when M=20. A 1:1 line is also included in Figure 6a. All mean CP_α values at various α levels plot close to the 1:1 line. This demonstrates again that the confidence level may be interpreted as the expected coverage proportion of the original and complete profile that falls within the corresponding CI profiles obtained from BCS, if this original profile can be measured. Additionally, for relatively large α values, the data are negatively skewed, similar to the random field data shown in Figure 2b, and the mean CP_α value is slightly below α.

Effect of the number of measurement data points (M) on CP_α

The BCS method was repeated with different number of measurement data points (M), namely, M = 10 to 60, with an increment of 10 points. These values correspond to measurement spacing between 30cm and 2m, and of fractions equal to 2% to about 12% of the complete profile. As M increases, more local variations of the original profile are captured by the reconstructed BCS mean profile, as shown by Wang and Zhao (2017). Additionally, as M increases, the bounds of the CI_{α} profiles become narrow and approach to the mean profile. This reflects that the statistical uncertainty is effectively reduced when more data points are available. In this section, the effect of M is evaluated on the coverage proportion of the original and complete profile that falls within the corresponding CI profiles obtained from BCS.

Figure 5 shows histograms of $CP_{50\%}$, $CP_{80\%}$ and $CP_{95\%}$ for three M values (i.e. M=20, 40 and 60). The mean $CP_{50\%}$, $CP_{80\%}$ and $CP_{95\%}$ values are shown in Figure 5d to 5f for M=40 as 0.54, 0.8, and 0.93, respectively. In Figure 5g to 5i, the mean $CP_{50\%}$, $CP_{80\%}$ and $CP_{95\%}$ values for M=60 are shown to be 0.48, 0.77, and 0.92, respectively. For M=20 and M=40, the mean $CP_{50\%}$ is slightly greater than 50% while the mean value for $CP_{95\%}$ is slightly less than 95%. Nonetheless, these mean CP_{α} values are quite close to their respective α values. On average a proportion α of all local variations of the original profile fall within the corresponding CI_{α} profiles, even when as few as M=20 points are used to reconstruct the mean and CI_{α} profiles, which is less than 4% of the total data. In Figure 5, it can be seen that the variability of the CP_{α} values decreases as M value increases. In addition, as previously shown for M=20 and for the full set of random field data, as α approaches unity the distribution develops a negative skewness. However, as can be seen for $CP_{80\%}$ and $CP_{95\%}$, as M increases, the distribution approaches to a normal distribution.

Similar to Figure 6a, Figures 6b and 6c show box-and-whiskers plots for CP_α with various α values when M=40 and 60, respectively. 1:1 lines are also include in these figures. As seen for M=20 in Figure 6a, the mean CP_α values at the α levels evaluated are close to the 1:1 line. In Figure 6 it is also evident that the variability of CP_α values decreases as M increases, e.g. see the size of the boxes in Figure 6. Figure 7 shows the mean values of $CP_{50\%}$, $CP_{80\%}$ and $CP_{95\%}$ for all values of M tested. Even though the statistical uncertainty is reduced with increasing M, the mean CP_α is not greatly affected and fluctuates around the α value. The relative difference between the average CP_α and α is less than 15% in all the cases tested. This demonstrates once again that the confidence level may be interpreted as the expected coverage proportion of the original and complete profile that falls within the corresponding BCS CI profiles.

Effect of correlation length on CP_α

To analyze the effect of the correlation length (λ_c) on CP_α results, new sets of RFSs are generated using a truncated KL expansion with different λ_c. Eight λ_c values were tested ranging from 0.1 to 10m to consider possible values of λ_c for soil properties reported in the literature (e.g. Phoon and Kulhawy 1999). For each RFS set, the BCS method was repeated for three values of M, namely M=20, 40 and 60. Figure 8 shows the mean CP_α results for all λ_c and M values tested. When λ_c is large (i.e. when there is a smoothly varying random field), the average CP_α tends to be greater than α, indicating that the statistical uncertainty reflected in the profiles for the bounds of CI_α is greater than the variations with depth. In other words, a relatively large proportion of many RFSs tested falls inside the corresponding CI_α profiles. In contrast, with small values of λ_c, which implies a very variable field, the average CP_α tends to be smaller than α, indicating that a relatively small proportion of the original profile falls inside the corresponding CI_α bounds. The difference between the average CP_α and α decreases as M increases, irrespective of whether the λ_c values used in the simulation are small or large. For λ_c values between 0.5m and 2m, which are common values for soil properties, the relative difference between the average CP_α and α is less than 15%. The BCS method is robust and performs satisfactorily for the possible range of λ_c values for soil properties reported in the literature. It is worth noting that it is very difficult to determine the correlation length (λ_c) in engineering practice due to the limited measurement data. Using the BCS method enables the need to determine the λ_c value to be bypassed and provides the best estimate and CI profiles for soil properties. In addition, note that, although an exponential correlation function is used as illustrative examples in this paper, the method proposed in the paper is general and equally applicable to other types of auto-correlation function, and the BCS method performs well for other types of auto-correlation function.

Illustrative example: Selection of effective friction angle profile

In this section, the BCS method is demonstrated using a set of real CPT data for selection of the characteristic value of the effective friction angle (ϕ'). BCS provides the best estimate profile of the effective friction angle and various CI profiles associated with various confidence levels. These CI profiles may be used by engineers to facilitate determination of the characteristic value profile in reliability-based design. To illustrate the proposed method, only some of the normalized tip resistance (q) values measured from CPT are used. First, the BCS method is applied to provide the best estimate and CI profiles of q. The coverage proportion of the BCS CI profiles is evaluated using the original and complete set of CPT data. Then a transformation model is used to relate the q profiles to ϕ' profiles. The effect of the transformation model uncertainty on the ϕ' profiles is also considered using Monte Carlo simulations. Note that the ϕ' profiles at various CI levels may be used by geotechnical engineers to facilitate selection of the ϕ' characteristic value in reliability-based design.

The CPT was performed on the Piedmont soils in Georgia Tech campus, Atlanta, in which an extensive program of in-situ and laboratory tests has been carried out for soil property determination (Mayne and Harris 1993). The BCS method is applied to the CPT data in the residual silty sand layer between the depths of 3.8 and 19.2m, approximately (Mayne and Harris 1993). Note that only one soil layer of residual silty sand is considered in this illustrative example. Stratification therefore is not needed here. However, for a profile with different soil layers, before application of the method proposed in this paper, stratification of soil layers shall be performed, if possible, using, for example, Bayesian method (Cao and Wang 2013; Wang et al. 2013,2014). In this layer, the cone tip resistance (q_c) ranges between 3.3MPa and 7.3MPa, and the soil has a loose to medium-dense relative density according to Meyerhof (1956). The soil has an average of 33% fines content, 8% clays and a median grain size (D50) of 0.14mm. Note that although CPT data is used here for illustration and validation, the BCS method really aims at the typical situation of sparsely measured data (e.g. SPT data or laboratory test data) in engineering practice.

The cone tip resistance is normalized by the square root of the vertical effective stress (σ'_{v0}) as follows: $q = (q_c/p_a)/\sqrt{\sigma'_{v0}/p_a}$, where p_a is the atmospheric pressure. The normalized tip resistance is shown in Figure 9a as a solid line. The BCS procedure is applied to 15 data points (i.e. M= 15), which represent a sampling interval of about 1m. These points are also shown in Figure 9a as open circles. The best estimate and the bounds of the 90% confidence interval ($CI_{90\%}$) obtained from BCS are shown in Figure 9a by a dashed and two dotted lines, respectively. The coverage proportion of the original CPT data within the $CI_{90\%}$ profiles is $CP_{90\%}$ = 85%, which is close to the expected value of 90%.

The effective friction angle (ϕ') is estimated using a correlation model from Kulhawy and Mayne (1990) as follows:

$$\phi' = 17.6 + 11\ \log \mathrm{q} \tag{9}$$

Figure 9b shows as a solid line the ϕ' profile obtained when applying Equation (9) to the original and complete set of CPT data. Similarly, shown as dashed and two dotted lines are the results when applying Equation (9) to the profiles of the best estimate and the bounds of the 90% CI obtained from the BCS procedure. For comparison, Figures 9b also includes lab test results from consolidated undrained triaxial compression tests that were performed using soil samples at different depths from this site (Mayne and Harris 1993). The mean ϕ' from the 13 triaxial test data points is about 35°, which is similar to the value obtained from BCS (i.e. 35.39°). However, the triaxial data present more variability than that shown by the BCS $CI_{90\%}$ profiles.

Note that Equation (9) was obtained by a semi-log regression on twenty data sets from different sites, which cover site condition similar to that at Georgia Tech campus, Atlanta. A total of 633 data points was used in the regression. Significant residual error over Equation (9) was reported, and the corresponding standard deviation of the residual error is 2.8° (Kulhawy and Mayne 1990). This residual error can be treated as the model uncertainty of Equation (9), and it may be included in Equation (9) as an additive zero-mean normally distributed random variable (ε_m). The ε_m in this example is modelled as a single random variable to represent a perfectly correlated nature of ε_m over depth. To account for both the model uncertainty and the BCS statistical uncertainty, Monte Carlo simulations were carried out to provide the best estimate and various CI profiles for the effective friction angle. Five thousand random samples of ε_m were generated in the simulations. Each ε_m sample was used together with Equation (9), and a complete q profile is reconstructed from BCS to generate a ϕ' profile, leading to 5000 friction angle profiles. Then, the $CI_{90\%}$ ϕ' profiles with model uncertainty was evaluated and shown in Figure 9c by two gray lines, together with those without model uncertainty using the same symbols in Figure 9b. The interval given by the two gray lines (i.e. with model uncertainty) is obviously much bigger than that given by two dotted lines (i.e. without model uncertainty). It is obvious that the model uncertainty has significant effect on the ϕ' profiles. The 13 ϕ' data points from triaxial tests are also included in Figure 9c. Eleven out of 13 data points (i.e. 11/13 = 85%) fall within the $CI_{90\%}$ ϕ' profiles. This is quite consistent with the statistical meaning of $CI_{90\%}$ ϕ' profiles that about 90% of data points are expected to fall within the corresponding bounds. The lower bound of $CI_{90\%}$ with both statistical and model uncertainty represents a 5% fractile of the ϕ' profile and might be selected as the characteristic value profile of ϕ' in reliability-based design, if the characteristic value is defined as the 5% fractile.

It is worth noting that the interpreted profile from the BCS method in this paper has meaning similar to the local estimation of a geotechnical property of interest at the location where a borehole was drilled (e.g. Honjo and Setiawan 2007; Honjo 2008). If global estimation of a geotechnical property (i.e. the geotechnical property within the whole site) is of interest (e.g. Honjo and Setiawan 2007; Honjo 2008), a perfect correlation in the horizontal direction may be assumed. Alternatively, the BCS method may be extended from

1D to 2D, and the perfect correlation assumption is not needed for 2D BCS method, which is currently under development and beyond the scope of this study.

Conclusions

This paper developed a statistical procedure to facilitate objective selection of geotechnical property characteristic value from spatially varying but sparsely measured data. The proposed procedure is based on the Bayesian compressive sampling (BCS) method, which is not only able to reconstruct the best estimate profile of a geotechnical property from sparse measurement data, but also able to provide confidence interval (CI) profiles for quantifying the statistical uncertainty associated with the interpretation. The quantified uncertainty in BCS has a clear statistical meaning: the corresponding confidence level for BCS CI is the expected coverage proportion (i.e. fraction) of the complete profile that falls within the CI, if all data points over the depth can be measured to provide the complete profile.

The statistical meaning of CI was firstly illustrated using random field data. When a large number of complete sets of random field samples (RFSs) are used, the expected coverage proportion (CP_α) for a confidence interval with a confidence level α (CI_α) is equal to α. In addition, when only a limited number of data points from the RFS are measured, the proposed BCS method can be used to reconstruct the best estimate and CI_α profiles of the complete set of RFS. It is shown that on average, the BCS CP_α is close to α even if only about 2% of the data points from the original and complete RFS are measured. As more data points are available the statistical uncertainty is reduced and the variability in CP_α also reduces, but the average value is only slightly affected. In addition, the effect of the correlation length (λ_c) of the random field on the average CP_α was also investigated. It is shown that the proposed method is robust and performs satisfactorily for the typical range of λ_c values for soil properties reported in the literature.

For geotechnical engineering applications, the complete set of data (i.e. a high-resolution measurement data profile over depth) is often not available, and the BCS method can be used to not only provide the best estimate profiles from sparse measurement data, but also offer various confidence interval profiles. To illustrate this, BCS was used to estimate an effective friction angle profile from sparse CPT data points in a real case history. Furthermore, the uncertainty in the transformation model that relates CPT data to effective friction angle can also be considered in the proposed method. It is shown that the effective friction angle CI profiles from the proposed method using sparse CPT data points are consistent with those from triaxial tests. Hence the best estimate and CI profiles from the proposed method may be used to facilitate an objective determination of geotechnical property characteristic values from sparse measurement data.

ACKNOWLEDGEMENT

The work described in this paper was supported by grants from the Research Grants Council of the Hong Kong Special Administrative Region, China (Project No. 9042331 (CityU 11225216) and Project No. 8779012 (T22-603/15N)). The financial support is gratefully acknowledged.

REFERENCES

AASHTO. 1998. *LRFD bridge design specifications*. Washington, D.C.

Ang, A.H.-S., and Tang, W.H. 2007. *Probability concepts in engineering: emphasis on applications to civil and environmental engineering*. New York: John Wiley and Sons.

Baecher, G.B., and Christian, J.T. 2003. *Reliability and Statistics in Geotechnical Engineering. Reliability and Statistics in Geotechnical Engineering*. http://doi.org/10.1198/tech.2005.s838

Becker, D.E. 2010. Testing in geotechnical design. *Geotechnical Engineering*, *41*(1).

Bond, A., and Harris, A. 2008. *Decoding Eurocode 7*. London and New York: Taylor & Francis.

Candès, E.J., Romberg, J.K., and Tao, T. 2006. Stable signal recovery from incomplete and inaccurate measurements. *Communications on Pure and Applied Mathematics*, *59*(8), 1207–1223. http://doi.org/10.1002/cpa.20124

Candès, E.J., and Wakin, M.B. 2008. An Introduction To Compressive Sampling. *IEEE Signal Processing Magazine*, *25*(2), 21–30. http://doi.org/10.1109/MSP.2007.914731

Cao, Z., and Wang, Y. 2013. Bayesian approach for probabilistic site characterization using cone penetration tests. *Journal of Geotechnical and Geoenvironmental Engineering*, 139(2), 267-276.

Cao, Z., and Wang, Y. 2014. Bayesian Model Comparison and Characterization of Undrained Shear Strength. *Journal of Geotechnical and Geoenvironmental Engineering*, *140*(6). http://doi.org/10.1061/(ASCE)GT.1943-5606.0001108.

Cao, Z., Wang, Y., and Li, D. 2016. Quantification of prior knowledge in geotechnical site characterization. *Engineering Geology*, *203*, 107–116. http://doi.org/10.1016/j.enggeo.2015.08.018

CEN 2004. *Eurocode 7: Geotechnical design — Part 1: General rules*, EN 1997−1:2004. European Committee for Standardization (CEN), Brussels, Belgium.

CHDBC 2014. Canadian Highway Bridge Design Code. CAN/CSAS614:2014, Canadian Standards Organization, Mississauga, Ontario, Canada.

Ching, J.Y. and Phoon, K.K. 2013a. Mobilized Shear Strength of Spatially Variable Soils Under Simple Stress States. *Structural Safety*, 41, 20-28.

Ching, J.Y. and Phoon, K.K. 2013b. Probability Distribution For Mobilized Shear Strengths of Spatially Variable Soils Under Uniform Stress States. *Georisk*, 7(3), 209-224.

Ching, J.Y., Phoon, K.K. and Kao, P.H. 2014. Probability Model for Overall Shear Strength of Spatially Variable Soils Under Uniform Stress States", *Journal of Engineering Mechanics*, ASCE, 140(3), 487-501

Ching, J.Y., Hu, Y.G. and Phoon, K.K. 2016a. On Characterizing Spatially Variable Shear Strength Using Spatial Average. *Probabilistic Engineering Mechanics*, 45, Jul 2016, 31-43

Ching, J.Y., Lee, S.W. and Phoon, K.K. 2016b. Undrained Strength for a 3D Spatially Variable Clay Column Subjected to Compression or Shear", *Probabilistic Engineering Mechanics*, 45, 127–139

Det Norske Veritas 2010. Statistical Representation of Soil Data. DNV-RP-C207.

De Veaux, R.D., Velleman, P.F., and Bock, D.E. 2014. *Intro Stats* (4th ed.). Pearson.

Efron, B., and Tibshirani, R.J. 1993. *An Introduction to the Bootstrap*. *Chapman & Hall/CRC*. Boca Raton, FL. http://doi.org/10.1111/1467-9639.00050

Fenton, G.A., and Naghibi, M. 2011. Geotechnical resistance factors for ultimate limit state design of deep foundations in frictional soils. *Canadian Geotechnical Journal*, **48**(11), 1742-1756. https://doi.org/10.1139/t11-068

Fenton, G.A., and Griffiths, D.V. 2008. *Risk Assessment in Geotechnical Engineering*. *Risk Assessment in Geotechnical Engineering*. http://doi.org/10.1002/9780470284704

Foucart, S., and Rauhut, H. 2013. *A Mathematical Introduction to Compressive Sensing*. *Applied and Numerical Harmonic Analysis*. http://doi.org/10.1007/978-0-8176-4948-7

Gong, W., Khoshnevisan, S., and Juang, C.H. 2014. Gradient-based design robustness measure for robust geotechnical design. *Canadian Geotechnical Journal*, **51**(11), 1331-1342. doi: 10.1139/cgj-2013-0428.

Ji, S., Xue, Y., and Carin, L. 2008. Bayesian compressive sensing. *IEEE Transactions on Signal Processing*, 56(6), 2346–2356. http://doi.org/10.1109/TSP.2007.914345

Honjo, Y. and Setiawan B. 2007. General and local estimation of local average and their application in geotechnical parameter estimations. *Georisk*, **1**(3), 167-176. http://dx.doi.org/10.1080/17499510701745960

Honjo, Y. 2008. General vs. local reliability based design in geotechnical engineering. In *Proceedings of the 4th Asian-Pacific Symposium on Structural Reliability and its Applications (APSSRA'08)*, Hong Kong, June 19-20. pp. 41-52.

Kulhawy, F.H., and Mayne, P.W. 1990. *Manual on Estimating Soil Properties for Foundation Design*. Ithaca, New York.

Li, D. Q., Shao, K.B., Cao, Z.J., Tang, X.S., and Phoon, K.K. 2016. A generalized surrogate response aided-subset simulation approach for efficient geotechnical reliability-based design. *Computers and Geotechnics*, 74, 88-101. https://doi.org/10.1016/j.compgeo.2015.12.010

Li, D.Q., Qi, X.H., Phoon, K.K., Zhang, L.M., and Zhou, C.B. 2014. Effect of spatially variable shear strength parameters with linearly increasing mean trend on reliability of infinite slopes. *Structural Safety*, 49, 45-55. doi: http://dx.doi.org/10.1016/j.strusafe.2013.08.005.

Marra, G., and Wood, S.N. 2012. Coverage Properties of Confidence Intervals for Generalized Additive Model Components. *Scandinavian Journal of Statistics*, *39*(1), 53–74. http://doi.org/10.1111/j.1467-9469.2011.00760.x

Mathworks. 2016. MATLAB – The language of technical computing.

Mayne, P.W., and Harris, D.E. 1993. *Axial load-displacement behavior of drilled shaft foundations in piedmont residuum*. McLeam, Virginia.

Meyerhof, G.G. 1956. Penetration tests and bearing capacity of cohesionless soils. *Journal of the Soil Mechanics and Foundations Division, ASCE*, *82*(SM1), 1–19.

Meyerhof, G.G. 1995. Development of geotechnical limit state design. *Canadian Geotechnical Journal*, *32*(1), 128–136. http://doi.org/10.1139/t95-010

Nychka, D. 1988. Bayesian confidence intervals for smoothing splines. *Journal of the American Statistical Association*, *83*(404), 1134–1143. http://doi.org/10.1080/01621459.1988.10478711

Orr, T.L.L. 2017. Defining and selecting characteristic values of geotechnical parameters for designs to Eurocode 7. *Georisk: Assessment and Management of Risk for Engineered Systems and Geohazards*, 11(1), 103–115. http://doi.org/10.1080/17499518.2016.1235711

Phoon, K.-K., and Ching, J. 2014. *Risk and Reliability in Geotechnical Engineering*. Boca Raton, FL: CRC Press, Taylor & Francis Group.

Phoon, K.-K., Huang, H.W., and Quek, S.T. 2005. Simulation of strongly non-Gaussian processes using Karhunen-Loeve expansion. *Probabilistic Engineering Mechanics*, *20*(2), 188–198. http://doi.org/10.1016/j.probengmech.2005.05.007

Phoon, K.-K., Huang, S.P., and Quek, S.T. 2002. Implementation of Karhunen-Loeve expansion for simulation using a wavelet-Galerkin scheme. *Probabilistic Engineering Mechanics*, *17*(3), 293–303. http://doi.org/10.1016/S0266-8920(02)00013-9

Phoon, K.-K., and Kulhawy, F.H. 1999. Characterization of geotechnical variability. *Canadian Geotechnical Journal*, *36*(4), 612–624. http://doi.org/10.1139/t99-038

Phoon, K.-K., Prakoso, W. A., Wang, Y., and Ching, J. 2016. Chapter 3 Uncertainty representation of geotechnical design parameters. In *Reliability Of Geotechnical Structures In Iso2394* (pp. 49–88). http://doi.org/10.1201/9781315364179-4

Reddy, S.C., and Stuedlein, A.W. 2017. Ultimate Limit State Reliability-Based Design of Augered Cast-in-Place Pile Considering Lower-Bound Capacities. *Canadian Geotechnical Journal*, doi: 10.1139/cgj-2016-0145.

Schneider, H.R., and Schneider, M.A. 2013. Dealing with uncertainties in EC7 with emphasis on determination of characteristic soil properties. *Modern Geotechnical Design Codes of Practice*, P. Arnold et al. (Eds.), ISO Press, 87-101.

Taboga, M. 2012. *Lectures on Probability Theory and Mathematical Statistics* (Second Edi). CreateSpace Independent Publishing Platform.

Vanmarcke, E.H. 1977. Probabilistic Modeling of Soil Profiles. *Journal of the Geotechnical Engineering Division*, *103*(11), 1227–1246.

Vick, S. 2002. *Degrees of Belief - Subjective Probability and Engineering Judgment,* ASCE Press.

Wahba, G. 1983. Bayesian "Confidence Intervals" for the Cross-validated Smooth Spline. *Journal of the Royal Statistical Society. Series B: Statistical Methodology*, 45(1), 133-150

Wang, Y., Akeju, O.V., and Cao, Z. 2016a. Bayesian Equivalent Sample Toolkit (BEST): an Excel VBA program for probabilistic characterisation of geotechnical properties from limited observation data. *Georisk: Assessment and Management of Risk for Engineered Systems and Geohazards*, 10(4), 251–268.

Wang, Y., and Aladejare, A.E. 2015. Selection of site-specific regression model for characterization of uniaxial compressive strength of rock. *International Journal of Rock Mechanics & Mining Sciences*, 75, 73–81.

Wang, Y., and Aladejare, A.E. 2016. Evaluating variability and uncertainty of Geological Strength Index at a specific site. *Rock Mechanics and Rock Engineering*, 49(9), 3559–3573.

Wang, Y., and Cao, Z. 2013. Probabilistic characterization of Young's modulus of soil using equivalent samples. *Engineering Geology*, 159, 106–118. http://doi.org/10.1016/j.enggeo.2013.03.017

Wang, Y., Cao, Z., and Li, D. 2016b. Bayesian perspective on geotechnical variability and site characterization. *Engineering Geology*, 203, 117–125. http://doi.org/10.1016/j.enggeo.2015.08.017

Wang, Y., and Zhao, T. 2016. Interpretation of soil property profile from limited measurement data : a compressive sampling perspective, *Canadian Geotechnical Journal*, 53(9), 1547-1559. http://doi.org/10.1139/cgj-2015-0545

Wang, Y., Huang, K., and Cao, Z. 2013. Probabilistic identification of underground soil stratification using cone penetration tests. *Canadian Geotechnical Journal*, 50(7), 766-776.

Wang, Y., Huang, K., and Cao, Z. 2014. Bayesian identification of soil strata in London clay. *Géotechnique*, 64(3), 239.

Wang, Y., and Zhao, T. 2017. Statistical interpretation of soil property profiles from sparse data using Bayesian compressive sampling. *Geotechnique*, http://dx.doi.org/10.1680/jgeot.16.P.143.

Zhang, J., and Ellingwood, B. 1994. Orthogonal Series Expansions of Random Fields in Reliability Analysis. *Journal of Engineering Mechanicsg*, 120(12), 2660–2667.

Figure Captions

Figure 1: N_s = 1000 sets of random field samples (RFSs) generated for soil property X (The 95% coverage proportion ($CP_{95\%}$) for the three RFS examples is indicated as title of each subplot)

Figure 2: Box-and-whiskers plot for the coverage proportion (CP_{α}) as a function of the confidence level (α) for different correlation length (λ_c): (a) 0.5m, (b) 2m and (c) 5m (Mean values are shown with circles; the median values are shown with a line inside the box; and the minimum and maximum values are shown with crosses)

Figure 3: Effect of the correlation length (λ_c) on CP_{α}: (a) Box plots for $CP_{50\%}$, $CP_{80\%}$ and $CP_{95\%}$; (b) Standard deviation of CP_{α} ($\sigma_{CP\alpha}$) as a function of α (The analytical solution for the case with no correlation (i.e. λ_c=0) is shown with a solid line)

Figure 4: Three simulated X profiles and those reconstructed from BCS using M = 20 measurement data points ***y***

Figure 5: Histograms of the coverage proportion (CP_{α}) for 50%, 80% and 95% confidence levels (The red vertical lines show the confidence level)

Figure 6: Box-and-whiskers plot for the coverage proportion (CP_{α}) of the original RFS profile within the given BCS CI under different M scenarios: (a) M = 20, (b) M = 40 and (c) M = 60

Figure 7: Effect of the number of measurement data points (M) on the mean CP_{α} values for confidence levels 50%, 80% and 95%.

Figure 8: Effect of the correlation length (λ_c) on the mean CP_{α} values

Figure 9: Results of illustrative example: estimation of effective friction angle ϕ' from normalized CPT tip resistance q: (a) Comparison between the original q profile and the q profile reconstructed from BCS (b) Best estimate and $CI_{90\%}$ profiles of ϕ' without consideration of model uncertainty ε_m (c) Best estimate and $CI_{90\%}$ profiles of ϕ' with consideration of model uncertainty ε_m

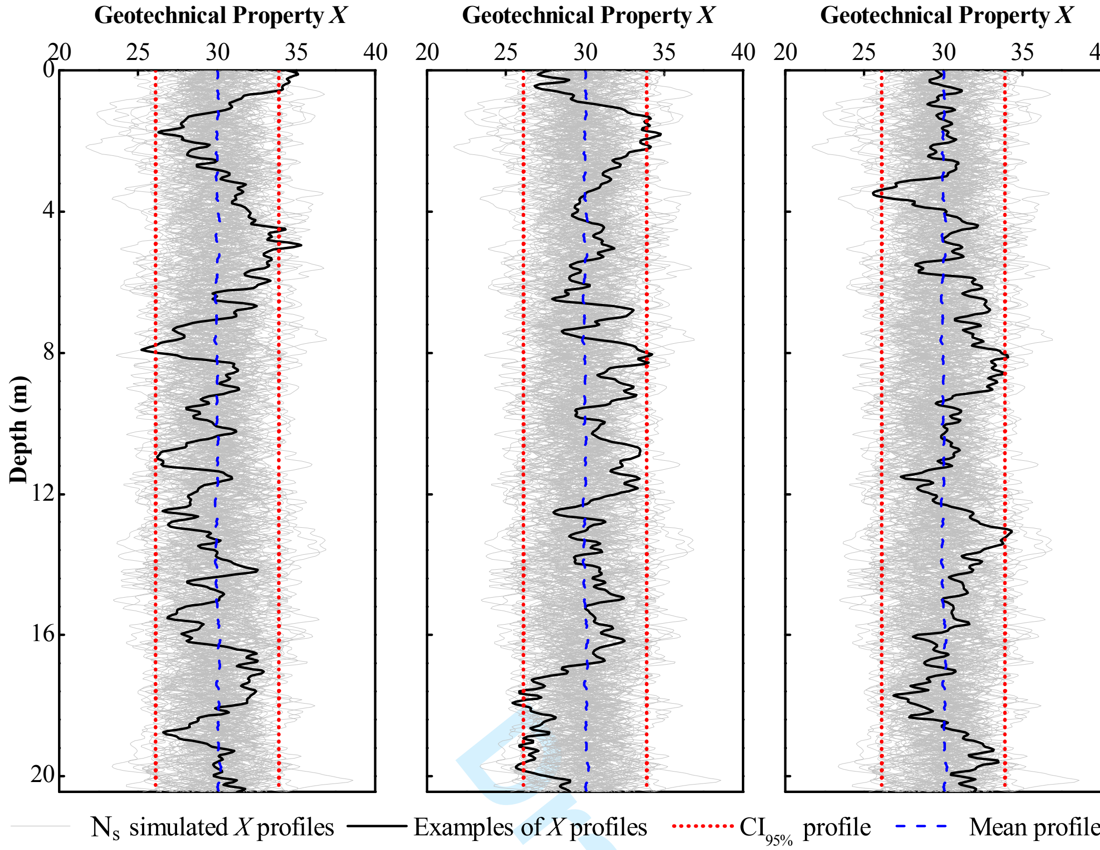

(a) $CP_{95\%}$=94.5% (b) $CP_{95\%}$=94.9% (c) $CP_{95\%}$=96.1%

Figure 1: N_s = 1000 sets of random field samples (RFSs) generated for soil property X (The 95% coverage proportion ($CP_{95\%}$) for the three RFS examples is indicated as title of each subplot)

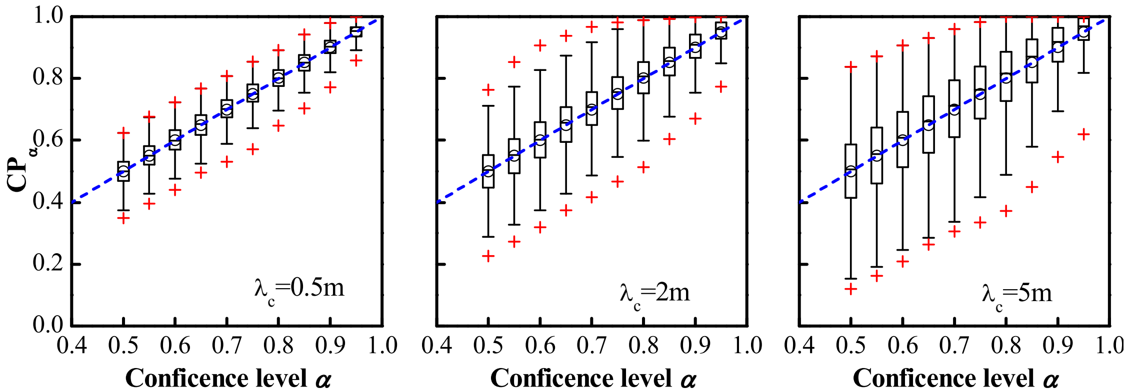

(a) (b) (c)

Figure 2: Box-and-whiskers plot for the coverage proportion (CP_α) as a function of the confidence level (α) for different correlation length (λ_c): (a) 0.5m, (b) 2m and (c) 5m (Mean values are shown with circles; the median values are shown with a line inside the box; and the minimum and maximum values are shown with crosses)

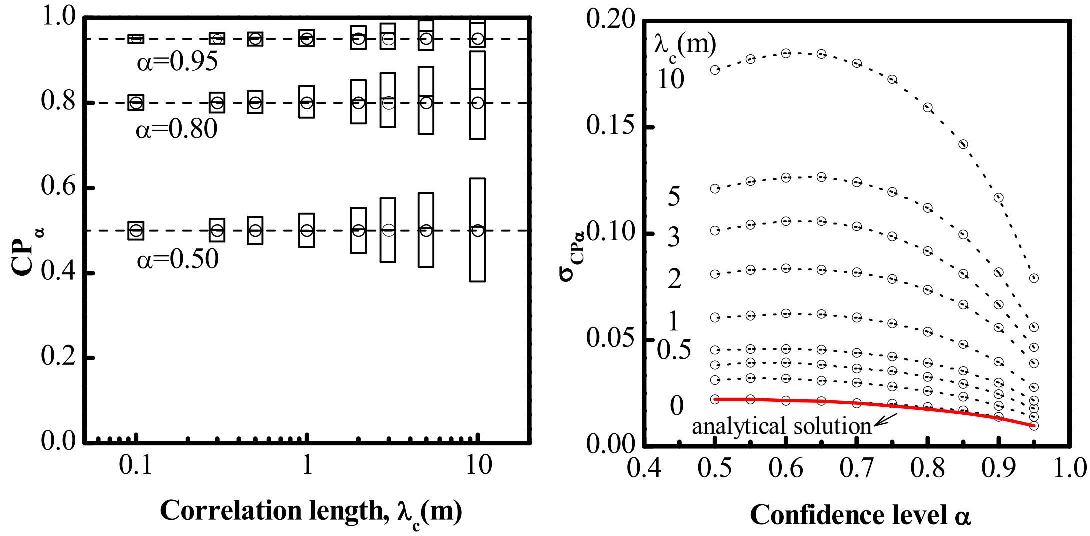

(a) (b)

Figure 3: Effect of the correlation length (λ_c) on CP_α: (a) Box plots for $CP_{50\%}$, $CP_{80\%}$ and $CP_{95\%}$; (b) Standard deviation of CP_α ($\sigma_{CP\alpha}$) as a function of α (The analytical solution for the case with no correlation (i.e. λ_c=0) is shown with a solid line)

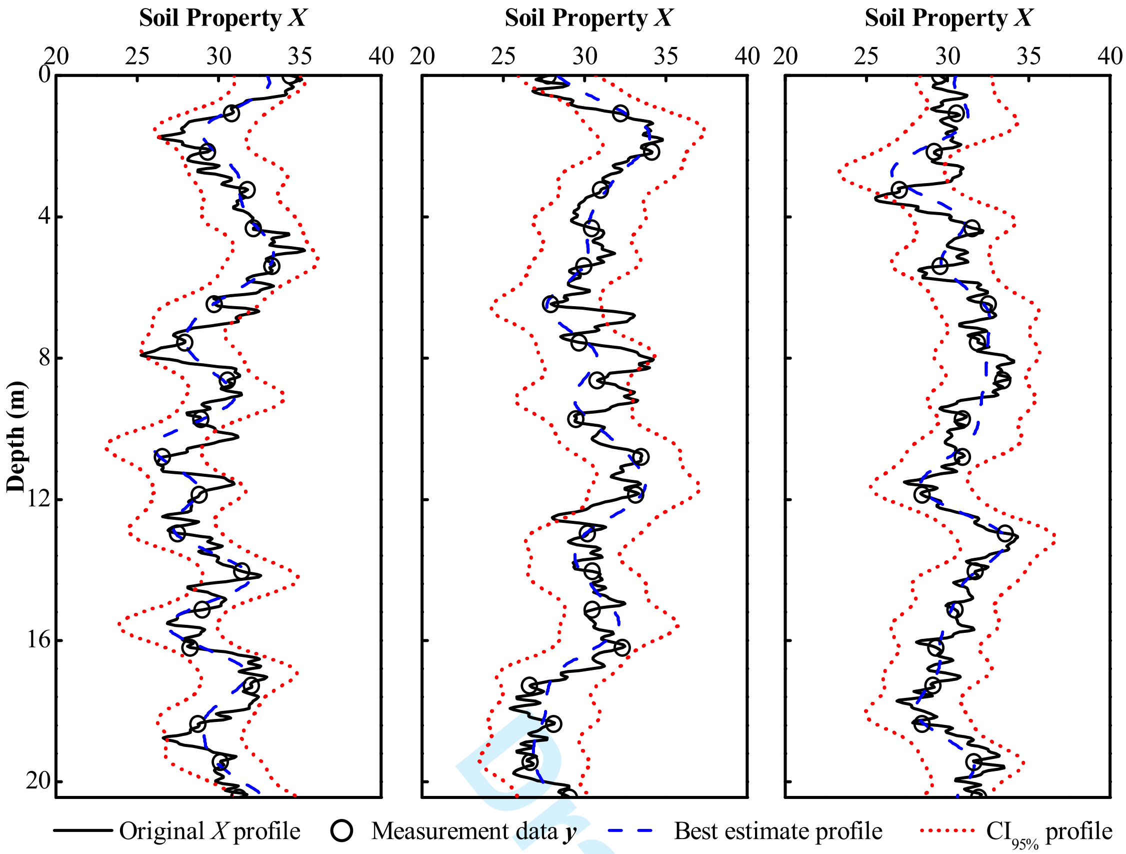

(a) $CP_{95\%}$=94.9% (b) $CP_{95\%}$=94.1% (c) $CP_{95\%}$=96.3%

Figure 4: Three simulated X profiles and those reconstructed from BCS using M = 20 measurement data points ***y***

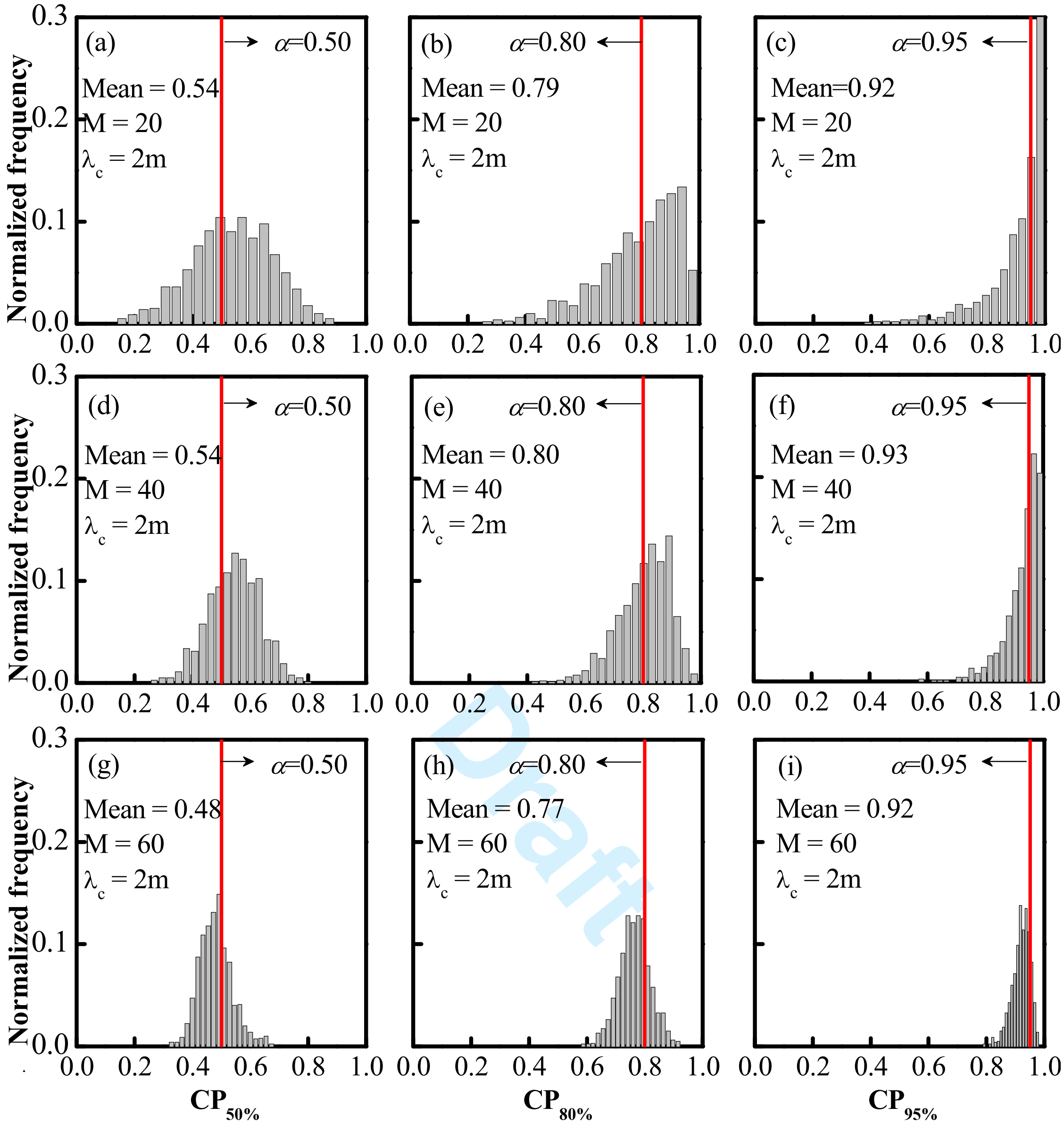

Figure 5: Histograms of the coverage proportion (CP_{α}) for 50%, 80% and 95% confidence levels (The red vertical lines show the confidence level)

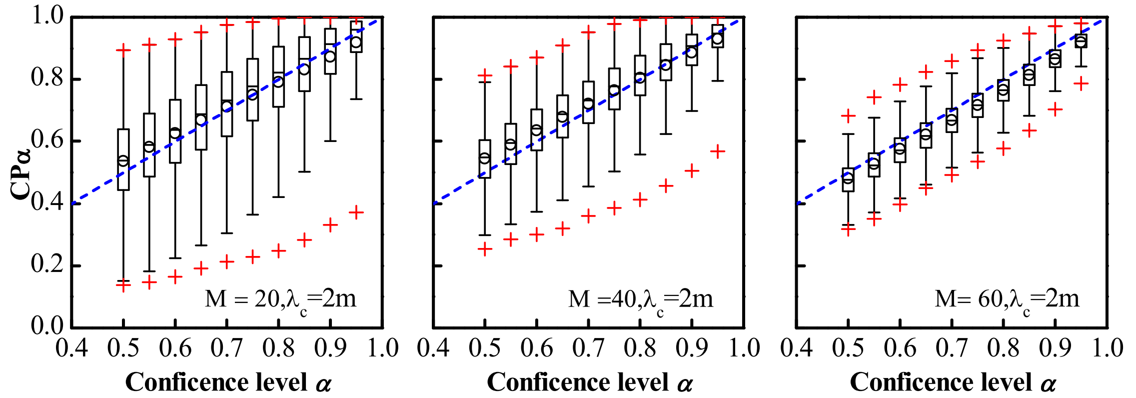

(a) (b) (c)

Figure 6: Box-and-whiskers plot for the coverage proportion (CP_α) of the original RFS profile within the given BCS CI under different M scenarios: (a) M = 20, (b) M = 40 and (c) M = 60

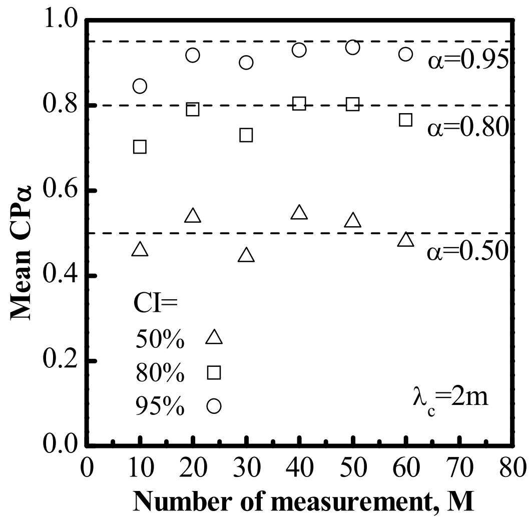

Figure 7: Effect of the number of measurement data points (M) on the mean CP_{α} values for confidence levels 50%, 80% and 95%.

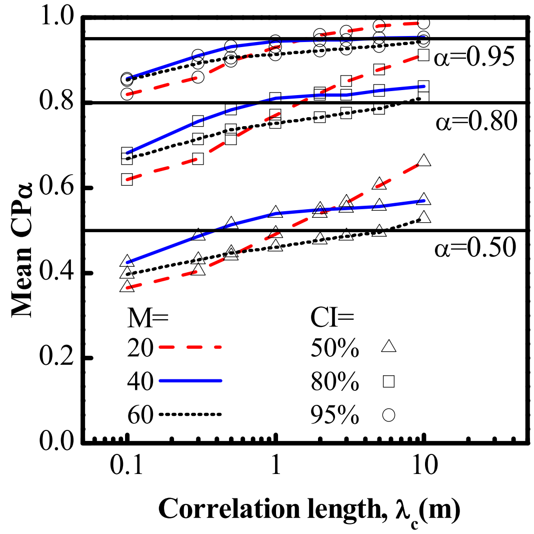

Figure 8: Effect of the correlation length (λ_c) on the mean CP_α values

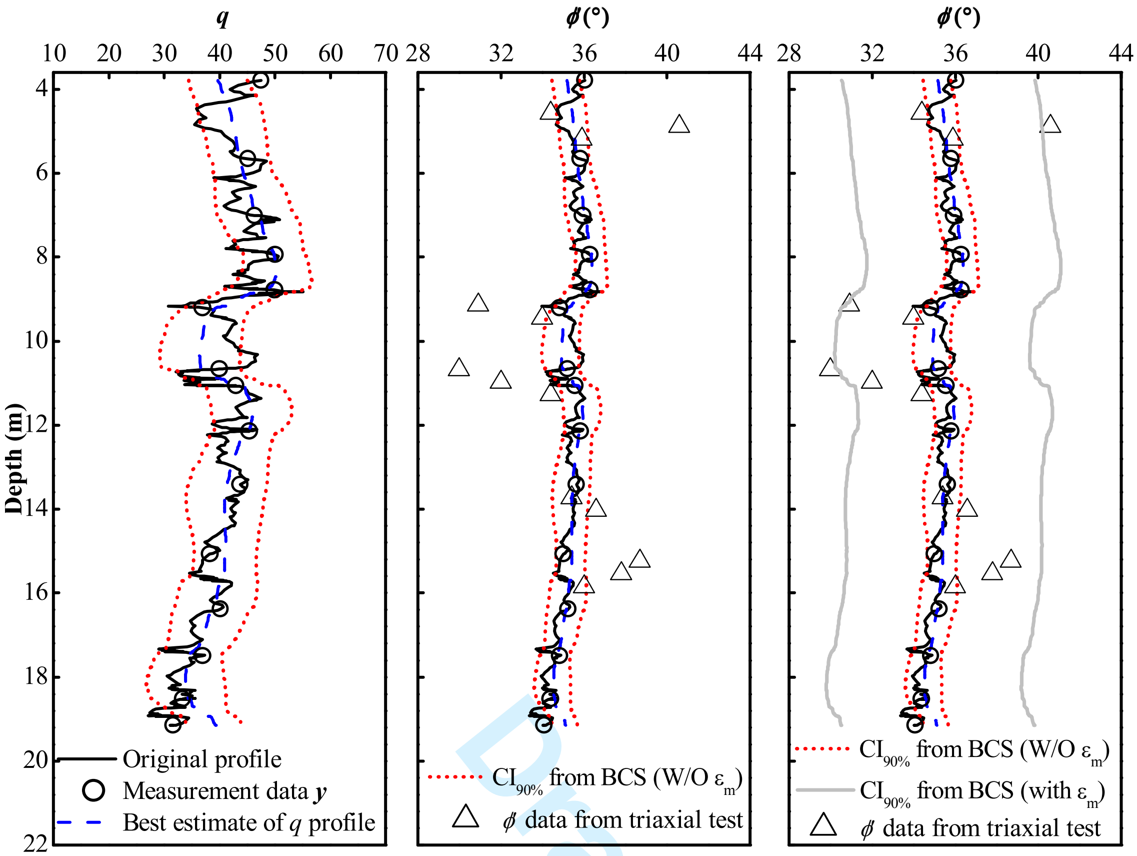

(a) (b) (c)

Figure 9: Results of illustrative example: estimation of effective friction angle ϕ' from normalized CPT tip resistance q: (a) Comparison between the original q profile and the q profile reconstructed from BCS (b) Best estimate and $CI_{90\%}$ profiles of ϕ' without consideration of model uncertainty ε_m (c) Best estimate and $CI_{90\%}$ profiles of ϕ' with consideration of model uncertainty ε_m